A balanced pyrimidine pool is required for optimal Chk1 activation to prevent ultrafine anaphase bridge formation

Simon Gemble, Géraldine Buhagiar-Labarchède, Rosine Onclercq-Delic, Denis Biard, Sarah Lambert, Mounira Amor-Guéret

▶ **To cite this version:**

Simon Gemble, Géraldine Buhagiar-Labarchède, Rosine Onclercq-Delic, Denis Biard, Sarah Lambert, et al.. A balanced pyrimidine pool is required for optimal Chk1 activation to prevent ultrafine anaphase bridge formation. Journal of Cell Science, 2016, 129 (16), pp.3167-3177. 10.1242/jcs.187781 . hal-02345992

HAL Id: hal-02345992
https://hal.science/hal-02345992

Submitted on 6 Dec 2020

HAL is a multi-disciplinary open access archive for the deposit and dissemination of scientific research documents, whether they are published or not. The documents may come from teaching and research institutions in France or abroad, or from public or private research centers.

L'archive ouverte pluridisciplinaire **HAL**, est destinée au dépôt et à la diffusion de documents scientifiques de niveau recherche, publiés ou non, émanant des établissements d'enseignement et de recherche français ou étrangers, des laboratoires publics ou privés.

© 2016. Published by The Company of Biologists Ltd | Journal of Cell Science (2016) 129, 3167-3177 doi:10.1242/jcs.187781

RESEARCH ARTICLE

A balanced pyrimidine pool is required for optimal Chk1 activation to prevent ultrafine anaphase bridge formation

Simon Gemble[1,2,3], Géraldine Buhagiar-Labarchède[1,2,3], Rosine Onclercq-Delic[1,2,3], Denis Biard[4], Sarah Lambert[1,2,3] and Mounira Amor-Guéret[1,2,3,*]

ABSTRACT

Cytidine deaminase (CDA) deficiency induces an excess of cellular dCTP, which reduces basal PARP-1 activity, thereby compromising complete DNA replication, leading to ultrafine anaphase bridge (UFB) formation. CDA dysfunction has pathological implications, notably in cancer and in Bloom syndrome. It remains unknown how reduced levels of PARP-1 activity and pyrimidine pool imbalance lead to the accumulation of unreplicated DNA during mitosis. We report that a decrease in PARP-1 activity in CDA-deficient cells impairs DNA-damage-induced Chk1 activation, and, thus, the downstream checkpoints. Chemical inhibition of the ATR–Chk1 pathway leads to UFB accumulation, and we found that this pathway was compromised in CDA-deficient cells. Our data demonstrate that ATR–Chk1 acts downstream from PARP-1, preventing the accumulation of unreplicated DNA in mitosis, and, thus, UFB formation. Finally, delaying entry into mitosis is sufficient to prevent UFB formation in both CDA-deficient and CDA-proficient cells, suggesting that both physiological and pathological UFBs are derived from unreplicated DNA. Our findings demonstrate an unsuspected requirement for a balanced nucleotide pool for optimal Chk1 activation both in unchallenged cells and in response to genotoxic stress.

KEY WORDS: Cytidine deaminase, Nucleotide pool, PARP-1, Chk1, Ultrafine anaphase bridges

INTRODUCTION

Genetic stability is ensured by complete genome duplication and balanced chromosome segregation. DNA replication errors are particularly deleterious because they can affect both DNA duplication and segregation during mitosis (Gelot et al., 2015). Replication stress is defined as any phenomenon affecting completion of the DNA replication program, including alterations to the initiation and elongation steps of DNA replication, conflicts between DNA replication and metabolic pathways, such as transcription and mRNA processing, nucleotide pool disequilibrium, and the overexpression or activation of oncogenes (Hills and Diffley, 2014; Lecona and Fernandez-Capetillo, 2014; Magdalou et al., 2014; Mazouzi et al., 2014). Such stress can jeopardize the completion of DNA replication and chromosome segregation, as illustrated by our previous studies showing that pyrimidine pool disequilibrium resulting from cytidine deaminase (CDA) deficiency is a source of replication stress and subsequent segregation defects (Chabosseau et al., 2011; Gemble et al., 2015). CDA is an enzyme of the pyrimidine salvage pathway that catalyzes the hydrolytic deamination of cytidine and deoxycytidine into uridine and deoxyuridine, respectively (Nygaard, 1986). CDA deficiency leads to intracellular dCTP accumulation, lowering the basal activity of poly(ADP-ribose) polymerase 1 (PARP-1), a multifunctional enzyme involved in many cellular processes, including in particular the response to DNA damage (Tallis et al., 2014). Decreases in PARP-1 activity lead to the under-replication of some 'difficult-to-replicate' loci in the genome, resulting in ultrafine anaphase bridge (UFB) formation (Gemble et al., 2015). UFBs reflect a defect in sister chromatid segregation during anaphase. They cannot be stained with conventional DNA dyes or antibodies against histones, but they can be detected with an antibody against Plk1-interacting checkpoint helicase (PICH, also known as ERCC6L), a protein recruited to UFBs (Baumann et al., 2007; Chan et al., 2007). UFBs are present in almost all cell lines and are, therefore, probably physiological structures (Chan et al., 2007). In the absence of exogenous stress, most are of centromeric origin, but some originate from common fragile sites or telomeres (Chan et al., 2007, 2009; Barefield and Karlsedar, 2012). UFB frequency often increases under constitutive or induced replication stress conditions (Chan et al., 2007, 2009).

CDA dysfunction has pathological implications, particularly in cancers, in which CDA activity might be either up- or downregulated, affecting the sensitivity of cancer cells to nucleotide analogs, such as gemcitabine (Ye et al., 2015; Zauri et al., 2015; Serdjebi et al., 2015). The importance of CDA defects and, more broadly, of pyrimidine pool disequilibrium, is illustrated by Bloom syndrome, a rare genetic disease displaying one of the strongest known correlations between chromosomal instability and an increase in cancer risk (German, 1997). In Bloom syndrome (DSA2) cells, the expression of genome instability markers results partly from pyrimidine pool disequilibrium resulting from a CDA defect. In particular, the supernumerary UFBs observed in Bloom syndrome cells result from CDA deficiency, which decreases basal PARP-1 activity (Gemble et al., 2015). Supernumerary UFBs are generated from unreplicated DNA. Thus, these observations raise questions about the mechanism underlying the persistence of unreplicated DNA during mitosis that we will need to resolve to improve our understanding of the pathological consequences of the incomplete genome replication caused by CDA defects.

We explored the potential role of one of the targets and partners of PARP-1, checkpoint kinase 1 (Chk1, also known as Chek1), in preventing the accumulation of unreplicated DNA during mitosis. Chk1, and its kinase, ataxia telangiectasia and Rad3-related (ATR), are key players in the regulation of the intra-S, S–M and G2–M

[1]Institut Curie, PSL Research University, UMR 3348, Unité Stress Génotoxiques et Cancer, Centre de Recherche, Orsay 91405, France. [2]CNRS UMR 3348, Centre Universitaire, Bât. 110, Orsay 91405, France. [3]Université Paris Sud, Université Paris Saclay, UMR3348, Centre Universitaire d'Orsay, Orsay 91405, France. [4]CEA, DSV, iMETI, SEPIA, 18, Route du Panorama. Bât. 60, BP6, Fontenay-aux-Roses Cedex 92265, France.

*Author for correspondence (mounira.amor@curie.fr)

M.A., 0000-0002-7713-167X

Received 14 February 2016; Accepted 27 June 2016

Journal of Cell Science

Journal of Cell Science (2016) 129, 3167-3177 doi:10.1242/jcs.187781

checkpoints (Sancar et al., 2004; Petermann and Caldecott, 2006; Eykelenboom et al., 2013; Smits and Gillespie, 2015). In response to genotoxic stress, the serine 317 and 345 residues of Chk1 are phosphorylated by ATR (Zhao and Piwnica-Worms, 2001; Liu et al., 2000), abolishing Chk1 auto-inhibition and allowing the subsequent activation of downstream checkpoints. Thus, activated Chk1 plays a major role in maintaining replication fork integrity and preventing cells from entering mitosis prematurely (Zuazua-Villar et al., 2014).

We show here that a lowering of basal PARP-1 activity levels in CDA-deficient cells compromises optimal Chk1 activation and decreases the efficiency of downstream checkpoints, leading to the accumulation of unreplicated DNA during mitosis and, ultimately, UFB formation. These results establish an unexpected link between the nucleotide pool and Chk1 activation and reveal a new role for Chk1 in preventing chromosome segregation defects.

RESULTS

The activation of Chk1 in response to genotoxic stress is reduced in CDA-deficient cells

PARP-1 catalyzes poly(ADP-ribosyl)ation (PARylation) by transferring ADP-ribose units from nicotinamide (NAD^+) onto diverse acceptor proteins (Luo and Kraus, 2012). The interaction of Chk1 with PAR is required for its efficient retention on DNA, and, thus, for its optimal activation (Min et al., 2013). We hypothesized that the lower levels of PARP-1 activity in CDA-deficient cells might decrease the stability of Chk1 on DNA and its activation. We analyzed the relative abundance of Chk1 in the chromatin-bound fractions from CDA-deficient or -proficient cells. GAPDH, BLM and histone 3 (H3) were used as loading controls for the cytoplasm, soluble nuclear and chromatin-bound fractions, respectively (Fig. 1A; Fig. S1A). Chk1 was found to be less abundant in the chromatin-bound fraction of PARP-1-deficient cells than in that of control cells. We thus confirmed that PARP-1 defects decrease the stability of Chk1 on DNA (Min et al., 2013) (Fig. S1A). Chk1 was also less abundant in the chromatin-bound fraction of CDA-deficient cells than in that of control cells (Fig. 1A). Additionally, PARP-1 was less abundant in the chromatin-bound fraction in the absence of CDA (Fig. 1A). Thus, CDA-deficient cells have small amounts of Chk1 bound to their DNA, suggesting that the activation of this protein might be weak in these cells.

We then investigated whether Chk1 activity was affected in CDA-deficient cells. Phosphorylation of the serine 317 residue of Chk1 is a classical marker of the activation of this protein (Zhao and Piwnica-Worms, 2001; Katsuragi and Sagata, 2004; Ng et al., 2004). However, this phosphorylation cannot be detected by standard immunoblotting in basal conditions without exogenous stress. We thus activated Chk1 by exposing CDA-deficient cells, or PARP-1-depleted cells as a control, to UVC (8 J/m^2) and analyzed Chk1 phosphorylation by immunoblotting. For CDA deficiency, we used two isogenic cell models, CDA-depleted HeLa cells and the corresponding control cells [HeLa-shCDA and HeLa-$Ctrl_{(CDA)}$, respectively] and Bloom syndrome cells expressing neither BLM nor CDA [BS-$Ctrl_{(BLM)}$] and the corresponding control cells expressing both BLM and CDA (BS-BLM) (Gemble et al., 2015). Chk1 phosphorylation levels were lower in PARP-1-deficient cells than in control cells (Fig. S1B), confirming that PARP-1 contributes to optimal Chk1 activation (Min et al., 2013). In CDA-deficient cells, Chk1 phosphorylation levels were 34% lower than those in CDA-expressing cells after exposure to UVC (Fig. 1B). These observations were reproduced by treating both HeLa-shCDA and BS cells with 25 nM CPT for 2 or 8 h (Fig. 1C; Fig. S1C).

CDA deficiency leads to an intracellular accumulation of dCTP (Chabosseau et al., 2011; Gemble et al., 2015). The addition of dC to the culture medium of CDA-proficient cells reproduces the increase in dCTP levels observed in CDA-deficient cells, mimicking CDA deficiency (Chabosseau et al., 2011; Gemble et al., 2015). We treated CDA-proficient and CDA-deficient cells with dC before CPT treatment. Lower levels of PARP-1 activity, resulting in lower levels of Chk1 activation, were observed in both cell types (Fig. 1D; Fig. S1E). Thus, increasing the size of the intracellular dCTP pool is sufficient to weaken the activation of PARP-1 and Chk1 in response to genotoxic stress and to decrease the activation of these proteins further in CDA-depleted cells. These data reveal an unexpected link between nucleotide pool disequilibrium and Chk1 activation.

The intracellular accumulation of dCTP resulting from CDA deficiency leads to a 30–50% decrease in basal PARP-1 activity (Gemble et al., 2015). We therefore investigated whether PARP-1 activity was also compromised in response to acute exposure to genotoxic stress, reflecting suboptimal Chk1 activation. We quantified PAR levels in CDA-deficient cells following treatment with either CPT or UVC, by immunofluorescence analysis with customized software for the automatic counting of PAR foci (Gemble et al., 2015). Basal PARP-1 activity in untreated CDA-deficient cells was weak, as previously reported (Gemble et al., 2015), but we also observed significantly fewer PAR foci in CDA-deficient cells treated with 25 nM CPT or exposed to 8 J/m^2 of UVC than in control cells exposed to the same stimuli (Fig. 1E,F; Fig. S1D). Thus, the PARP-1 activity of CDA-deficient cells is weak not only in basal conditions, but also in response to genotoxic stress.

These data indicate that, in CDA-deficient cells subjected to genotoxic stress, the intracellular accumulation of dCTP decreases PARP-1 activity, thereby compromising optimal Chk1 activation.

In response to genotoxic stress, the efficiency of the Chk1-dependent S-phase and G2–M checkpoints is compromised in the absence of CDA

Our data showing that Chk1 activation was compromised in CDA-deficient cells subjected to genotoxic stress led us to explore the possible functional consequences for downstream cell-cycle delays in these cells. Chk1 plays a key role in the S- and G2–M-phase checkpoints in response to DNA damage (Smits and Gillespie, 2015; Segurado and Tercro, 2009). S-phase checkpoint activation suppresses replication origin firing and stabilizes stalled replication forks, leading to a decrease in DNA synthesis and an accumulation of cells in S-phase (Smits and Gillespie, 2015; Segurado and Tercero, 2009). Thus, to quantify S-phase checkpoint efficiency, we first measured DNA synthesis in CDA-deficient cells and control cells by exposing them to UVC (8 J/m^2) and adding EdU to the cell culture medium for one hour, either immediately after UVC treatment or 16 h later. Then we analyzed EdU incorporation into DNA by flow cytometry, to determine the relative proportions of DNA synthesis after UVC treatment, with decreases considered to reflect S-phase checkpoint efficiency. DNA synthesis had decreased one hour after UVC treatment in all cells analyzed (Fig. 2A; Fig. S2A), but PARP-1-depleted cells displayed higher levels of DNA synthesis than PARP-1-expressing cells, as previously reported (Min et al., 2013) (Fig. S2A). Similarly, CDA-depleted cells displayed higher levels of DNA synthesis one hour after UVC exposure than CDA-expressing cells (Fig. 2A). DNA synthesis had returned to basal levels 16 h after UVC exposure in both cell types, confirming that the decrease in DNA synthesis resulted from transient checkpoint activation rather than cell death (Fig. 2A;

Journal of Cell Science

Journal of Cell Science (2016) 129, 3167-3177 doi:10.1242/jcs.187781

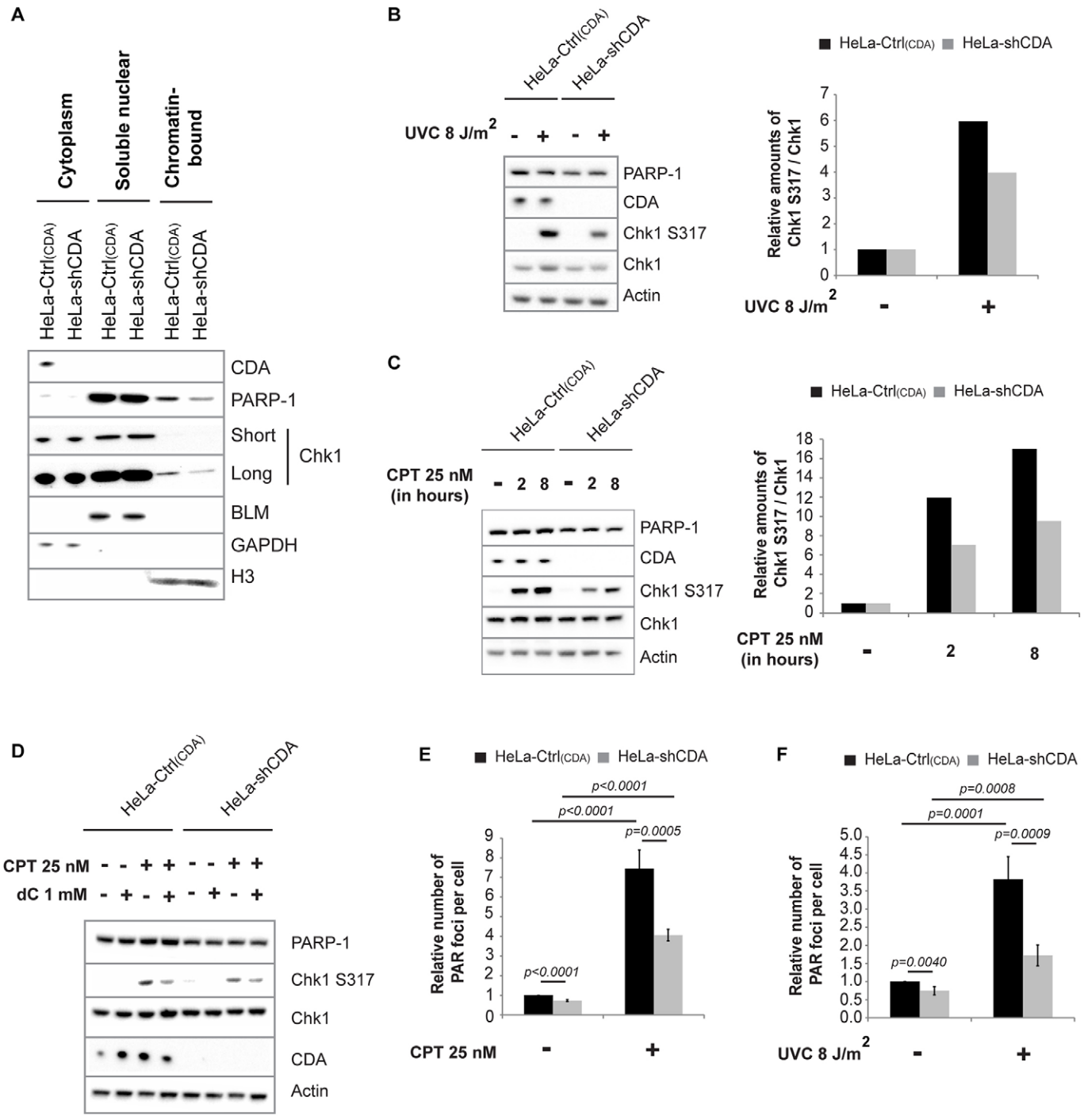

Fig. 1. CDA deficiency compromises PARP-1 and Chk1 activation after genotoxic stress. (A) Representative immunoblot of subcellular fractions from HeLa-Ctrl$_{(CDA)}$ or HeLa-shCDA cell lines. GAPDH, BLM and H3 proteins were used as loading controls for the cytoplasmic, nuclear and chromatin-bound fractions, respectively. (B) Left panel, representative immunoblot of HeLa-Ctrl$_{(CDA)}$ or HeLa-shCDA cells left unexposed or exposed to 8 J/m^2 UVC. Right panel, corresponding quantification of the amount of Chk1 S317 normalized against Chk1. (C) Left panel, representative immunoblot of HeLa-Ctrl$_{(CDA)}$ or HeLa-shCDA cells left untreated or treated with 25 nM CPT for 2 or 8 h. Right panel, corresponding quantification of the amount of Chk1 S317 normalized against Chk1. (D) Representative immunoblot of HeLa-Ctrl$_{(CDA)}$ or HeLa-shCDA cells left untreated or treated with 1 mM dC for 8 h, with or without treatment with 25 nM CPT for 2 h. (E,F) Relative numbers of PAR foci in HeLa-Ctrl$_{(CDA)}$ and HeLa-shCDA cells (E) left untreated or treated with 25 nM CPT for 8 h (n=4, >530 cells analyzed) or (F) left unexposed or exposed to 8 J/m^2 UVC (n=4, >500 cells analyzed). The error bars indicate the mean±s.d. Statistical significance was calculated with Student's t-test.

Fig. S2A). The inhibition of Chk1 by CHIR-124, its specific inhibitor (Tse et al., 2007), abolished the decrease in DNA synthesis one hour after UVC treatment, in both CDA-deficient and CDA-proficient cells (Fig. S2B). The efficiency of Chk1 inhibition was confirmed by the accumulation of Cdc25A protein, the degradation of which is dependent on Chk1 activity (Boutros and Ducommun, 2008) (Fig. S2C). These data confirmed that the decrease in DNA synthesis in response to UVC resulted from Chk1-dependent

Journal of Cell Science

Journal of Cell Science (2016) 129, 3167-3177 doi:10.1242/jcs.187781

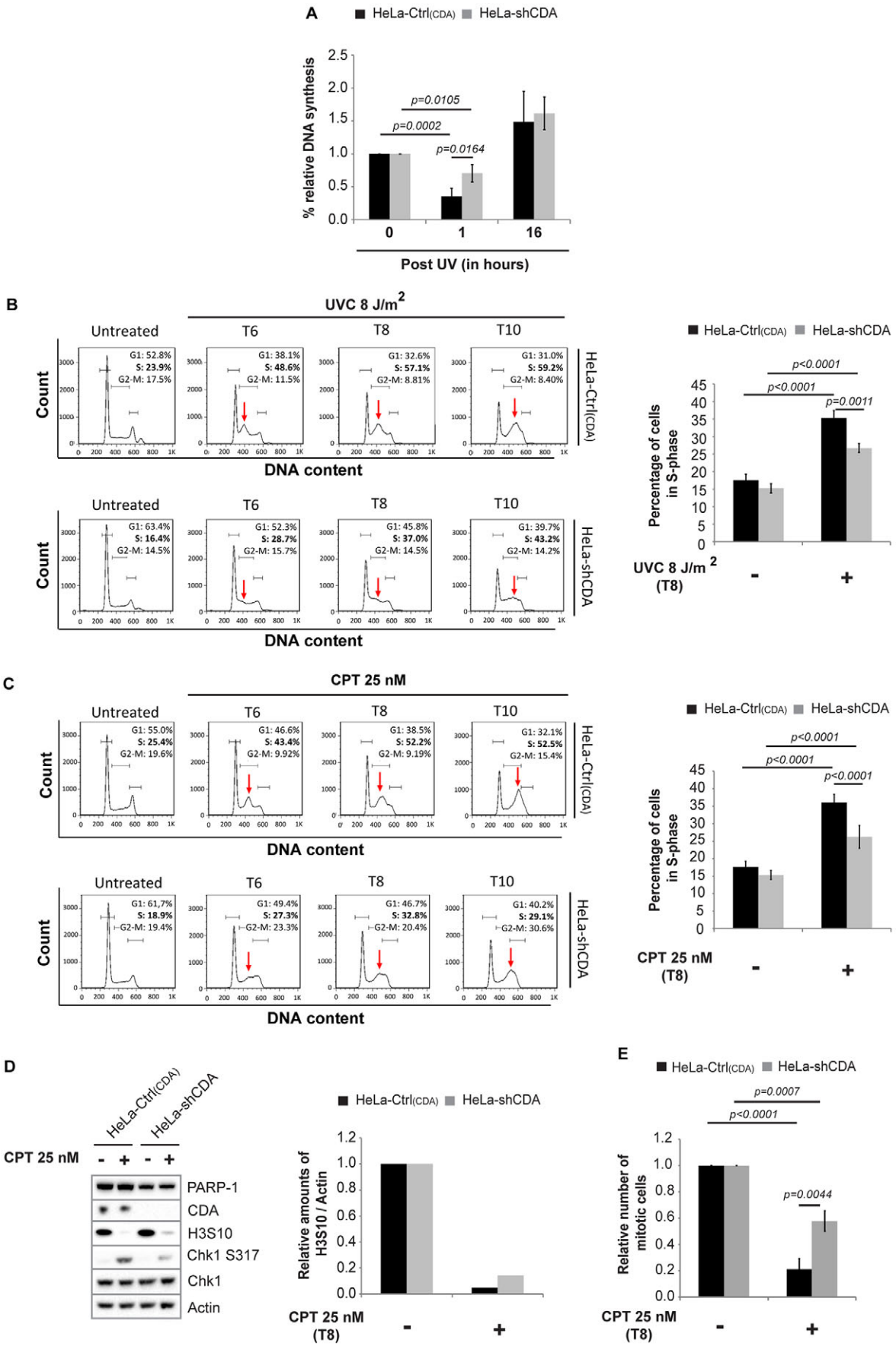

Fig. 2. See next page for legend.

Journal of Cell Science

Journal of Cell Science (2016) 129, 3167-3177 doi:10.1242/jcs.187781

Fig. 2. CDA deficiency jeopardizes the efficiency of Chk1-dependent checkpoints. (A) Percentage relative DNA synthesis in HeLa-Ctrl$_{(CDA)}$ or HeLa-shCDA cell lines unexposed or exposed to 8 J/m^2 UVC (n=3). (B) Left panel, representative cell cycle distribution of HeLa-Ctrl$_{(CDA)}$ and HeLa-shCDA cells unexposed or exposed to 8 J/m^2 UVC. Right panel, percentage HeLa-Ctrl$_{(CDA)}$ and HeLa-shCDA cells in S-phase 8 h after exposure to 8 J/m^2 UVC (n=3). (C) Left panel, representative cell cycle distribution for HeLa-Ctrl$_{(CDA)}$ and HeLa-shCDA cells left untreated or treated with 25 nM CPT. Right panel, percentage of HeLa-Ctrl$_{(CDA)}$ or HeLa-shCDA cells in S-phase after being left untreated or treated with 25 nM CPT for 8 h (n=7). Red arrows in B,C indicate peak representing cells in S-phase. (D) Left panel, representative immunoblot of HeLa-Ctrl$_{(CDA)}$ and HeLa-shCDA cells left untreated or treated with 25 nM CPT for 8 h. Right panel, corresponding quantification of the amount of H3S10 normalized against actin. (E) Relative number of mitotic cells in HeLa-Ctrl$_{(CDA)}$ and HeLa-shCDA cells left untreated or treated with 25 nM CPT for 8 h (n=3; >1500 cells analyzed). Error bars represent the mean±s.d. Statistical significance was calculated with Student's t-test.

activation of the S-phase checkpoint, and revealed a lower efficiency of this checkpoint in CDA-deficient cells.

Further support for these conclusions was provided by an analysis of the cell cycle distribution of cells with and without CDA expression, at various times after exposure to genotoxic stress. The increase in the percentage of cells in S-phase (red arrows in left panels, Fig. 2B,C) in response to CPT or UVC treatment was significantly smaller in CDA-deficient cells (Fig. 2B,C, right panels) than in control cells, and entry into S-phase was inhibited by CHIR-124 treatment (Fig. S2D,E).

Thus, Chk1-dependent S-phase checkpoint activation was less efficient in the absence of CDA, reducing the inhibition of DNA synthesis and resulting in the accumulation of smaller number of cells in S-phase, in response to a genotoxic stress.

We also observed that more CDA-deficient cells than control cells accumulated in the G2–M phase (Fig. 2B,C, left panels). We therefore investigated the efficiency, in CDA-deficient cells, of the G2–M checkpoint, which prevents entry into mitosis in the presence of DNA damage (Dai and Grant, 2010). We quantified histone 3 with a phosphorylated serine 10 residue (H3S10), a specific marker of mitosis, after CPT treatment. The H3S10 signal was still visible eight hours after treatment with 25 nM CPT in CDA-deficient cells, whereas it was not detectable in control cells (Fig. 2D). Thus, a higher percentage of cells enter mitosis, despite DNA damage, in the absence of CDA. Consistent with these results, analysis of the mitotic index revealed a significantly higher percentage of CDA-deficient cells than of control cells in mitosis after CPT treatment (Fig. 2E). These results were confirmed by flow cytometry analysis, which showed the percentage of H3S10-positive cells after CPT treatment to be significantly higher for CDA-deficient cells than for CDA-proficient cells (Fig. S2F). Thus, G2–M checkpoint activation was less efficient in CDA-deficient cells.

These results show that the low levels of Chk1 activation in CDA-deficient cells decrease the efficiency of the DNA damage-induced S and G2–M checkpoints, leading to a premature passage of cells from S-phase to mitosis despite the presence of DNA damage and, potentially, under-replicated DNA, particularly at late-replicating sequences. As CDA-deficient cells contain smaller amounts of DNA-bound Chk1, we hypothesized that the low levels of basal Chk1 activity contributed to the formation of UFB-containing unreplicated DNA in the absence of exogenous genotoxic treatment.

The ATR–Chk1 pathway prevents supernumerary UFB formation

The excess UFB formation in CDA-deficient cells is a marker of unreplicated DNA accumulation during mitosis, but the origin of the basal UFBs remains unclear (Gemble et al., 2015). Chk1 inhibition triggers the premature entry of S-phase cells into mitosis before the completion of DNA replication (Zuazua-Villar et al., 2014), and we observed low levels of Chk1 activation in CDA-deficient cells (Fig. 1), which are known to present supernumerary UFBs (Gemble et al., 2015). We therefore hypothesized that Chk1 inhibition might favor the accumulation of unreplicated DNA during mitosis, and, consequently, UFB formation. We treated CDA-deficient or CDA-proficient cells with Chk1 inhibitor CHIR-124 or with VE-821, an inhibitor of ATR, the kinase that activates Chk1 in response to DNA damage (Zhao and Piwnica-Worms, 2001), and analyzed UFB frequency in anaphase cells. Increases in H3S10 expression in both CDA-proficient and CDA-deficient cells treated with VE-821 revealed premature entry into mitosis, confirming ATR inhibition (Fig. 3A). We found that the inhibition of Chk1 or ATR led to an increase in UFB frequency in CDA-proficient cells, to levels similar to those in CDA-deficient cells, whereas it had no effect on UFB frequency in CDA-deficient cells (Fig. 3B–D). These results demonstrate the importance of the ATR–Chk1 pathway for preventing supernumerary UFB formation. As the inhibition of ATR or Chk1 had no effect on UFB frequency in CDA-deficient cells, these results suggest that CDA and ATR–Chk1 prevent UFB formation through the same pathway. Our previous results showing that CDA-deficient cells display a constitutive activation of both γH2AX and Chk2 (Gemble et al., 2015) led us to investigate the possible involvement of the ATM–Chk2 pathway in supernumerary UFB formation in these cells. We analyzed UFB frequency in CDA-deficient cells and in CDA-proficient cells left untreated or treated with KU55933, a specific inhibitor of ATM (Hickson et al., 2004). As expected, the level of phosphorylation of the threonine 68 residue of Chk2 by ATM was much lower in the KU55933-treated cells, confirming the inhibition of ATM (Fig. S3A). ATM inhibition had no effect on UFB frequency in CDA-expressing cells or CDA-deficient cells (Fig. S3B), demonstrating an absence of ATM–Chk2 pathway involvement in UFB formation.

We have shown that the treatment of CDA-deficient cells with very low doses of CPT (2 pM) is sufficient to increase basal levels of PARP-1 activity to those observed in untreated CDA-proficient cells. Such a restoration of PARP-1 activity is sufficient to prevent the accumulation of unreplicated DNA and, thus, supernumerary UFBs (Gemble et al., 2015). We investigated whether the ATR–Chk1 pathway acted downstream from PARP-1 to prevent UFB formation in CDA-deficient cells, by determining whether the suppression of UFB formation by low-doses of CPT required a functional ATR–Chk1 pathway. In CDA-proficient cells, the inhibition of Chk1 or ATR stimulated UFB formation, independently of treatment with low doses of CPT (Fig. 3E,F, black bars). In CDA-deficient cells, low doses of CPT abolished the formation of supernumerary UFBs, unless Chk1 or ATR was inhibited (Fig. 3E,F, gray bars). Thus, PARP-1 activation prevents the formation of supernumerary UFBs in CDA-deficient cells in an ATR–Chk1-dependent manner.

These findings demonstrate that the accumulation of unreplicated DNA and, thus, of supernumerary UFBs in the absence of CDA is caused by low levels of PARP-1 activity, resulting in a weakening of ATR–Chk1-dependent checkpoints.

Prolongation of the cell cycle prevents UFB formation in both CDA-proficient cells and CDA-deficient cells

The results presented above suggest that the low levels of ATR–Chk1 activity observed in the absence of CDA lead to the premature entry of S-phase cells with partially replicated

Journal of Cell Science (2016) 129, 3167-3177 doi:10.1242/jcs.187781

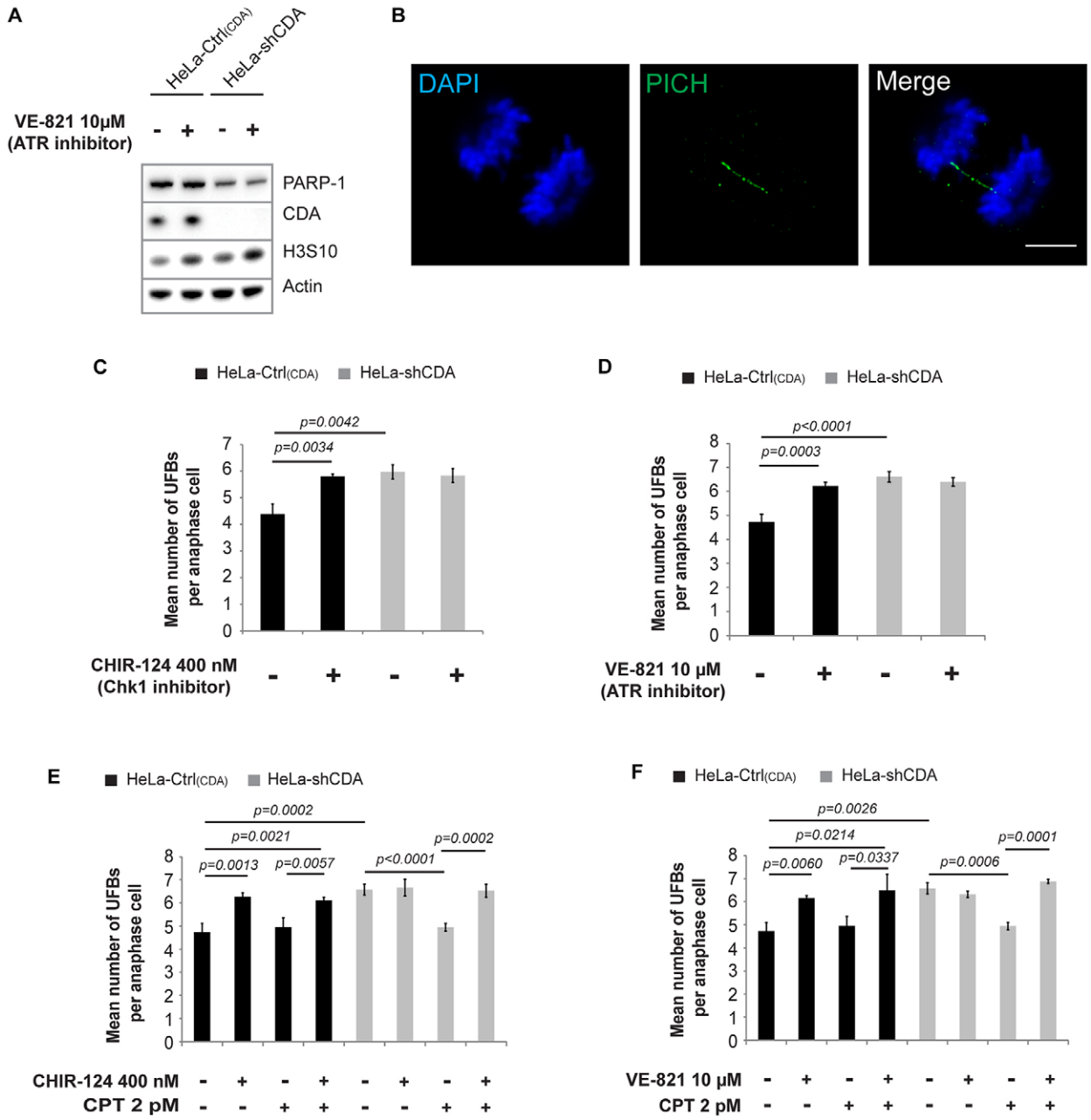

Fig. 3. Chk1 inhibition promotes UFB formation in CDA-expressing cells. (A) Representative immunoblot of HeLa-Ctrl$_{(CDA)}$ and HeLa-shCDA cell lines left untreated or treated with 10 μM VE-821 for 8 h. (B) Representative deconvoluted *z*-projection immunofluorescence images of PICH-positive UFBs in HeLa-Ctrl$_{(CDA)}$ anaphase cells. DNA was visualized with DAPI (in blue). UFBs were stained with an anti-PICH antibody (in green). Scale bar: 5 μm. (C,D) Mean number of UFBs per anaphase cell in HeLa-Ctrl$_{(CDA)}$ and HeLa-shCDA cells left untreated or treated for 8 h with (C) 400 nM CHIR-124 or (D) 10 μM VE-821 (n=3; >100 anaphase cells analyzed). (E,F) Mean number of UFBs per anaphase cell in HeLa-Ctrl$_{(CDA)}$ and HeLa-shCDA cells left untreated or treated with 2 pM CPT for 8 h, with or without (E) 400 nM CHIR-124 or (F) 10 μM VE-821 (n=3; >95 anaphase cells analyzed). Error bars represent the mean±s.d. Statistical significance was calculated with Student's *t*-test.

chromosomes into G2–M, resulting in an excess of UFB-containing unreplicated DNA.

These data led us to investigate whether delaying entry into mitosis might allow cells to complete DNA replication before entering mitosis, thereby preventing UFB formation. The treatment of cells with low doses of RO-3306, a cyclin-dependent kinase 1 (Cdk1) inhibitor, or with volasertib, a polo-like kinase 1 (Plk1) inhibitor, delays entry into mitosis (Eykelenboom et al., 2013; Rudolph et al., 2009; Raab et al., 2015).

Cells were treated with either RO-3306 or volasertib, leading to an increase in the percentage of cells in the S and G2 phases (Fig. 4A,B), and an increase in cyclin B1 levels (Fig. 4C,D). This delaying of entry into mitosis was associated with a significant decrease in the frequencies of unreplicated centromeres and UFBs during mitosis, not only in CDA-deficient cells, but also in CDA-proficient cells (Fig. 4E–G; Fig. S4A,B). We checked that the cells in anaphase had previously experienced extended S and G2 phases by adding

Journal of Cell Science

Journal of Cell Science (2016) 129, 3167-3177 doi:10.1242/jcs.187781

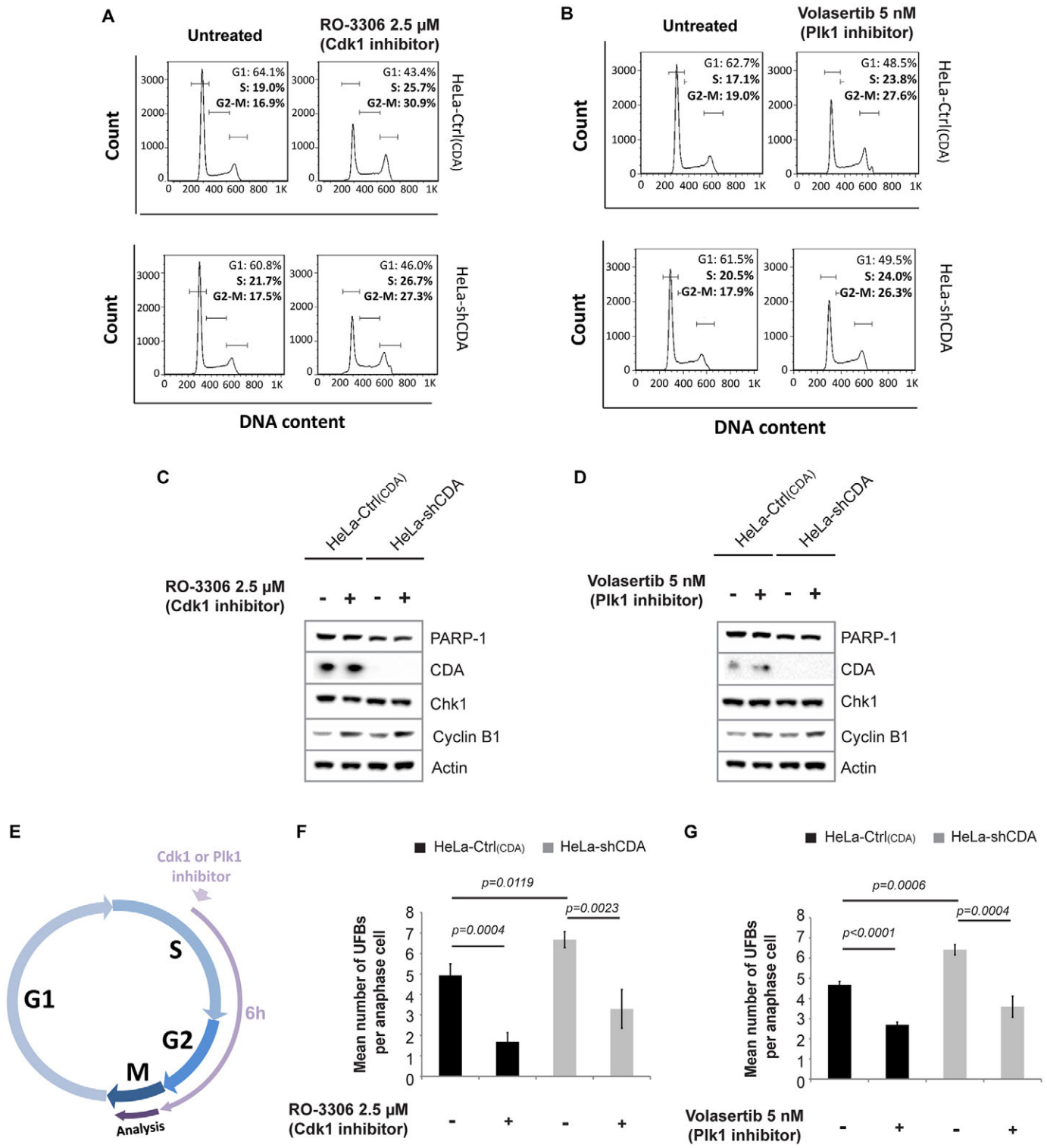

Fig. 4. Promoting the completion of DNA replication prevents UFB formation. (A,B) Representative distribution in the cell cycle of HeLa-Ctrl$_{(CDA)}$ and HeLa-shCDA cells left untreated or treated for 6 h with (A) 2.5 µM RO-3306 or (B) 5 nM volasertib. (C,D) Representative immunoblot of HeLa-Ctrl$_{(CDA)}$ and HeLa-shCDA cells left untreated or treated for 6 h with (C) 2.5 µM RO-3306 or (D) 5 nM volasertib. (E) Schematic representation of the protocol for the treatment with Cdk1 or Plk1 inhibitors; all cells analyzed during mitosis were treated with Cdk1 or Plk1 inhibitors during S and G2 phases. (F,G) Mean number of UFBs per anaphase cell in HeLa-Ctrl$_{(CDA)}$ and HeLa-shCDA cells left untreated or treated for 6 h with (F) 2.5 µM RO-3306 or (G) 5 nM volasertib (n=4; >95 anaphase cells analyzed). Error bars represent the mean±s.d. Statistical significance was calculated with Student's t-test.

EdU to cell cultures one hour before RO-3306 treatment for the labeling of S-phase cells (Fig. S4C). All the mitotic cells analyzed were EdU-positive, confirming that cells in anaphase with low UFB frequencies had previously gone through extended S and G2 phases (Fig. S4D). Finally, given that PICH is regulated by Plk1 and Cdk1 (Baumann et al., 2007), we

Journal of Cell Science

Journal of Cell Science (2016) 129, 3167-3177 doi:10.1242/jcs.187781

checked that low doses of RO-3306 had no effect on the location of PICH at the centromeres of mitotic cells (Fig. S4E), confirming that the decrease in UFB frequency did not result from a change in PICH distribution.

These data indicate that delaying entry into mitosis is sufficient to promote the completion of DNA replication, thereby preventing the formation of basal and supernumerary UFBs. These findings suggest that all UFBs result from the accumulation of unreplicated DNA during mitosis.

DISCUSSION

We recently reported a new mechanism by which excess cellular dCTP, resulting from CDA deficiency, partially inhibits the basal activity of PARP-1, leading to the under-replication of some 'difficult-to-replicate' loci, resulting in UFB formation during mitosis (Gemble et al., 2015). Here, we identify a downstream target of PARP-1, the ATR–Chk1 pathway, dysfunctions of which lead to an accumulation of UFB-containing under-replicated DNA. Our findings reveal that pyrimidine pool disequilibrium jeopardizes Chk1 activation. We demonstrate that the intracellular accumulation of dCTP resulting from CDA deficiency reduces PARP-1 activity and, thus, Chk1 activation, thereby weakening the S and G2–M checkpoints. We suggest that this decrease in checkpoint efficiency promotes the accumulation of unreplicated DNA during mitosis, leading to excess UFB formation (Fig. 5).

We found that PARP-1 activity levels were low in CDA-deficient cells not only in basal conditions, but also in response to genotoxic stress. The intracellular accumulation of dCTP thus also impairs the enhancement of PARP-1 activation. PARP-1 interaction with DNA is necessary for its activation (Langelier and Pascal, 2013); the low levels of PARP-1 in the chromatin-bound fraction from CDA-deficient cells studied here suggest that increases in dCTP concentration disturb the interaction of PARP-1 with DNA, thereby compromising its subsequent activation.

We also found that Chk1 levels were low in the chromatin-bound fraction from CDA-deficient cells. These results are consistent with those of a previous study showing that PAR, supplied by PARP-1, interacts with Chk1, promoting its efficient retention on DNA and its optimal activation (Min et al., 2013). Thus, the small amounts of DNA-bound Chk1 probably result from the low level of PARP-1 recruitment to DNA, and, thus, from insufficient Chk1–PAR interaction. As expected, the low levels of DNA-bound Chk1 affected the activation of this protein in response to genotoxic stress, confirming that optimal PARP-1 activity is required for the correct enhancement of Chk1 activation. Culturing cells with deoxycytidine, which is known to increase intracellular levels of dCTP and to decrease PARP-1 activity (Gemble et al., 2015), was sufficient to reproduce the cellular phenotype associated with CDA-deficiency; poor Chk1 activation in response to genotoxic stress. These data reveal an unexpected requirement for a balanced nucleotide pool to ensure optimal Chk1 activation.

The weakening of downstream checkpoint efficiency is a direct consequence of the low levels of Chk1 activity in the absence of CDA. Indeed, CDA-deficient cells present incomplete S and G2–M checkpoint activation in response to genotoxic stress. These data confirm our previous findings that, in response to UVC, BLM-deficient cells display partial escape from the G2–M cell cycle checkpoint (Ababou et al., 2002). The failure of CDA-deficient cells to activate the S and G2–M checkpoints optimally in response to genotoxic stress might account for the accumulation of DNA damage observed directly by electron microscopy in these cells and indirectly detected through the constitutive activation of the γH2AX–Chk2 pathway (Gemble et al., 2015).

Our findings suggest that insufficient Chk1 activity allows cells with partially replicated chromosomes to enter mitosis, leading to the formation of UFB-containing under-replicated DNA in CDA-deficient cells. We would thus expect to reproduce this phenotype by inhibiting Chk1 or its sensor kinase, ATR. We found that ATR–Chk1 pathway inhibition resulted in excess UFB formation in CDA-proficient cells but not in CDA-deficient cells. These results not only support our hypothesis, but also indicate that CDA, PARP-1, Chk1 and ATR act through the same pathway to prevent the accumulation of unreplicated DNA, and, thus, the formation of supernumerary UFBs, during mitosis.

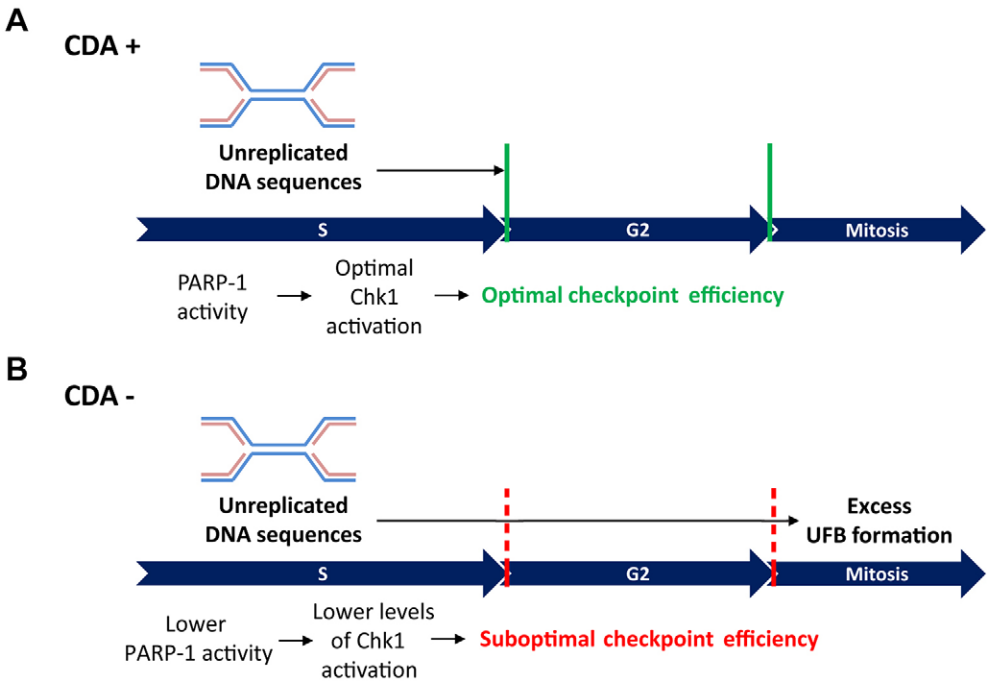

Fig. 5. Balanced pyrimidine pool ensures optimal Chk1 activation, preventing the formation of supernumerary UFBs. (A) In CDA-proficient cells, basal PARP-1 activity ensures optimal Chk1 activation, promoting optimal checkpoint efficiency and preventing the accumulation of unreplicated DNA at the onset of mitosis. (B) In CDA-deficient cells, low levels of PARP-1 activity compromise optimal Chk1 activation, decreasing checkpoint efficiency and promoting the entry into mitosis of cells containing unreplicated DNA and, consequently, excessive UFB formation.

Journal of Cell Science

Consistent with this finding, we demonstrated that restoring PARP-1 activity by treating CDA-deficient cells with very low doses of CPT did not prevent UFB formation if either Chk1 or ATR was inhibited.

The ATR–Chk1 pathway prevents S-phase cells from entering mitosis prematurely (Eykelenboom et al., 2013; Zuazua-Villar et al., 2014). Thus, the low levels of Chk1 activation in CDA-deficient cells might promote premature entry into mitosis, before the completion of DNA replication, thereby accounting for the excess of UFB-containing unreplicated DNA formation. Consistent with this hypothesis, we showed that delaying entry into mitosis led to a decrease in the frequencies of unreplicated centromeres and UFBs during mitosis, not only in CDA-deficient cells, but also in CDA-proficient cells. These results indicate that all UFBs are derived from unreplicated DNA sequences, regardless of CDA status. We suggest that UFBs can be considered markers of the accumulation of under-replicated DNA during mitosis. This raises the question of the significance of UFBs, as these structures have been detected in all cells tested, whether primary or transformed, under physiological conditions (Chan et al., 2007). The MUS81–EME1 and ERCC1 nucleases and mitotic DNA synthesis have been reported to process unreplicated DNA sequences in mitosis (Gemble et al., 2015; Ying et al., 2013; Naim et al., 2013; Bergoglio et al., 2013), preventing excess UFB formation. All the experimental strategies used to date have succeeded only in reducing UFB numbers to the threshold UFB frequency in control cells, a physiological level. Our results are the first to show that delaying entry into mitosis is sufficient to reduce physiological UFB frequency in control cells to below this threshold. We therefore suggest that UFB formation is an additional mechanism for processing unreplicated DNA during mitosis, in situations in which processing by nucleases or mitotic DNA synthesis has failed.

MATERIALS AND METHODS

Cell culture and treatments

Cell lines were cultured in DMEM supplemented with 10% FCS. BS-$Ctrl_{(BLM)}$ and BS-BLM cells were obtained and cultured as previously described (Chabosseau et al., 2011). HeLa-$Ctrl_{(CDA)}$ and HeLa-shCDA cells were obtained and cultured as previously described (Gemble et al., 2015). HeLa-$Ctrl_{(PARP\text{-}1)}$ and HeLa-shPARP-1 cells were cultured as previously described (Gemble et al., 2015).

Deoxycytidine (dC) was provided by Sigma Aldrich (D0779); Camptothecin (CPT) was provided by Sigma Aldrich (C9911); CHIR-124 was provided by Selleckchem (S2683); MK-1775 was provided by Selleckchem (S1525); VE-821 was provided by Selleckchem (S8007); volasertib was provided by Selleckchem (S2235); KU55933 was provided by Selleckchem (S1092) and RO-3306 was provided by Calbiochem (217699). Drugs were added to the cell culture medium at the following concentrations: dC, 1 mM; camptothecin, 2 pM or 25 nM; CHIR-124, 400 nM; VE-821, 10 µM; volasertib, 5 nM; KU55933, 10 µM; RO-3306, 2.5 µM.

For the UVC experiment, we used the cells to seed six-well plates, which were incubated for 24 h before UVC exposure. Exponentially growing cells were irradiated in 1 ml PBS. Plates were placed uncovered under a UVC lamp (G25T8 germicidal lamp, Sankyo Denki, Japan) operating at 0.02 mW/cm^2. Dosimetry was performed with a VLX 3W radiometer (Vilber Lourmat, France) equipped with a 254 nm probe.

All cells were routinely checked for mycoplasma infection.

Western blot analysis and antibodies

Cells were lysed in 8 M urea, 50 mM Tris HCl, pH 7.5 and 150 mM β-mercaptoethanol, sonicated and heated at 75°C for 10 min. Samples (equivalent of 2×10^5 cells) were subjected to electrophoresis in NuPAGE Novex 4–12% Bis-Tris pre-cast gels (Life Technologies). The procedures used for gel electrophoresis and immunoblotting have been described elsewhere (Gemble et al., 2015), except that a Bio-Rad ChemiDoc XRS+ camera was used for detection. Primary and secondary antibodies used were as follows: rabbit anti-BLM antibody (1:5000; ab2179 from Abcam); rabbit anti-CDA antibody (1:500; ab56053 from Abcam); rabbit anti-β-actin antibody (1:10,000; Cat no. A2066 from Sigma); rabbit anti-PARP-1 antibody (1:4000; ALX-210-302 from Enzo Life Sciences); rabbit anti-Chk1 (1:500; sc-8408 from Santa Cruz Biotechnology); rabbit anti-Chk1-S317 (1:500; 2344 from Cell Signaling); mouse anti-H3S10 (1:500; 14955 from Abcam); mouse anti-Cdc25A (1:500; sc-7389 from Santa Cruz Biotechnology); rabbit anti-H3 (1:5000; ab1791 from Abcam); rabbit anti-cyclin-B1 (1:1000; sc-245 from Santa Cruz Biotechnology); mouse anti-GAPDH (1:500; G8795 from Sigma); rabbit anti-Chk2 (1:500; 2662 from Cell Signaling); rabbit anti-Chk2-T68 (1:500; 2661 from Cell Signaling); rabbit anti-H2AX (1:500; 2595 from Cell Signaling); rabbit anti-H2AX-S139 (1:500; 2577 from Cell Signaling) and horseradish-peroxidase-conjugated goat anti-rabbit-IgG or goat anti-mouse-IgG (1:5000; Cat nos. sc-2054 and sc-2055, respectively, from Santa Cruz Biotechnology).

Mitotic index

We used 4×10^5 HeLa cells to seed the wells of a six-well plate. The cells were left untreated or were treated as mentioned in the figures. They were then washed in PBS and fixed by incubation in 4% paraformaldehyde for 20 min. Nuclear DNA was detected by mounting slides in ProlongH Gold Antifade reagent supplemented with DAPI (Invitrogen), making it possible to distinguish between mitotic and interphase cells. Images were acquired with a Leica DM RXA microscope equipped with a motorized *xy* stage, using a 40× PlanApo N.A. 1.25 objective and a CoolSNAP HQ interline CCD camera (Photometrics). For each slide, a mosaic of 10×10 partly overlapping images was acquired with a Metamorph software (Molecular Devices) routine developed in-house. Image collections were assembled into a mosaic with the 'Stitching 2D/3D' plugin32 (available from http://fly.mpi-cbg.de/~preibisch/software.html) for ImageJ software (National Institutes of Health, Bethesda, Maryland). Mitotic index was calculated by measuring the percentage of mitotic cells in each mosaic.

Immunofluorescence microscopy

Immunofluorescence staining and analysis were performed as previously described (Gemble et al., 2015). Primary and secondary antibodies used were as follows: rabbit anti-PICH (1:150; H00054821-D01P from Abnova); mouse anti-PICH (1:400; H00054821-M01 from Abnova); human anti-CREST (1:100; 15-234-0001 from Antibodies Inc); goat anti-human Alexa Fluor 633 (1:500; A21091 from Life Technologies); goat anti-rabbit Alexa Fluor 555 (1:500; A21429 from Life Technologies); goat anti-mouse Alexa Fluor 555 (1:500; A21050 from Life Technologies). Cell images were acquired with a 3D deconvolution imaging system consisting of a Leica DM RXA microscope equipped with a piezoelectric translator (PIFOC; PI) placed at the base of a 63× PlanApo N.A. 1.4 objective, and a CoolSNAP HQ interline CCD camera (Photometrics). Stacks of conventional fluorescence images were collected automatically at a *z*-distance of 0.2 mm (Metamorph software, Molecular Devices). Images are presented as maximum intensity projections, generated with ImageJ software, from stacks deconvolved with an extension of Metamorph software (Savino et al., 2001). EdU incorporation into DNA was visualized with the Click-it EdU imaging kit (C10338 from Life Technologies), according to the manufacturer's instructions. EdU was incubated with cells at a concentration of 10 µM for 1 h.

Poly(ADP)-ribose immunofluorescence

We used 4×10^5 HeLa cells to seed the wells of a six-well plate. The cells were left untreated or were treated as mentioned in the figures. They were then washed in cold PBS on ice and fixed by incubation in a 1:1 (vol/vol) mixture of methanol and acetone for 10 min on ice. After three washes in PBS–Tween (0.05%), cells were incubated overnight at 4°C with a mouse anti-PAR antibody [1:500; generously provided by Valérie Schreiber (Illuzzi et al., 2014)]. The cells were washed three times with PBS–Tween (0.05%) and incubated with a goat anti-mouse Alexa-Fluor-555-conjugated

antibody (1:500; A21050 from Life Technologies) for 2 h. After two washes in PBS–Tween (0.05%), cells were mounted on slides with Prolong Gold with DAPI (P36931 from Life Technologies). Cell images were acquired with a 3D deconvolution imaging system consisting of a Leica DM RXA microscope equipped with a piezoelectric translator (PIFOC; PI) placed at the base of a 63× PlanApo N.A. 1.4 objective, and a CoolSNAP HQ interline CCD camera (Photometrics). Stacks of conventional fluorescence images were collected automatically at a *z*-distance of 0.2 mm (Metamorph software, Molecular Devices). Images are presented as maximum intensity projections, generated with ImageJ software, from stacks deconvolved with an extension of Metamorph software (Savino et al., 2001). PAR foci per nucleus were counted by a customized macro using a semi-automated procedure, as follows: the nucleus stack was first smoothed using a median filter (radius 5), the user defined an intensity value as a threshold (one value for all experiments); a mask was then generated and transferred onto the stack of foci so that only foci in nuclei were analyzed. A top-hat filter was applied to the result to eliminate local background and facilitate the segmentation process, based on a simple threshold (user-defined value). Finally, the macro counted and characterized foci. At least 500 nuclei were analyzed for each condition.

Flow cytometry

Cells were detached by treatment with Accutase (Sigma), immediately washed in 1× PBS, fixed in 70% ethanol and stored at −20°C overnight. They were then washed in 1× PBS and 1× staining buffer (554656 from BD Pharmingen). DNA content was visualized by incubating the cells with 7-AAD (559925 from BD Pharmingen) for 15 min at room temperature.

DNA synthesis was visualized with the Click-iT EdU Alexa Fluor 647 Flow Cytometry Assay Kit (C-10419 from ThermoFisher Scientific), according to the manufacturer's instructions. EdU was used at a concentration of 10 µM for 1 h.

Cell cycle analysis or EdU incorporation was visualized with a FACSCalibur (Becton-Dickinson), by analyzing 50,000 cells per condition. Data were then analyzed with FlowJo software (Tree Star Inc.).

p-Histone 3 staining

Cells were detached by treatment with Accutase (Sigma), immediately washed in 1× PBS, fixed in 70% ethanol and stored at −20°C overnight. They were then washed two times in 1× PBS and incubated for 1 h with an anti-histone 3 (phospho S10) antibody (1:200; 14955 from Abcam) in Stain Buffer (554656 from BD Pharmingen). Cells were washed in 1× PBS and incubated for 30 min with a goat anti-mouse Alexa-Fluor-633-conjugated antibody (1:500; A21052 from Life Technologies), propidium iodide (P4864 from Sigma) and RNAse A (R6513 from Sigma) in Stain Buffer at 37°C.

P-Histone 3 staining and DNA content were visualized with a FACSCalibur (Becton-Dickinson), by analyzing 10,000 cells per condition. Data were then analyzed with FlowJo software (Tree Star Inc.).

Subcellular fractionation

Subcellular analysis was performed with the Subcellular Protein Fractionation Kit for Cultured Cells (78840 from ThermoFisher Scientific), according to the manufacturer's instructions.

Statistical analysis

At least three independent experiments were carried out to generate each dataset and the statistical significance of differences was calculated with Student's *t*-test, as indicated in the figure legends.

Acknowledgements

We acknowledge the assistance of Marie-Noëlle Soler (PICT-IBiSA, Institut Curie, Orsay) and Charlène Lasgi (Flow Cytometry platform, Institut Curie, Orsay). We thank V. Schreiber and Jean-Christophe Amé (Institut de recherche de l'Ecole de biotechnologie de Strasbourg, Strasbourg) for providing us with anti-PAR antibodies.

Competing interests

The authors declare no competing or financial interests.

Author contributions

S.G. performed the experiments, participated in the design of the experiments and data analysis, generated the figures and wrote the manuscript. G.B.-L., R.O.-D. and D.B. performed experiments. S.L. contributed to data analysis and preparation of the manuscript. M.A.-G. designed the experiments, analyzed the data and wrote the manuscript.

Funding

This work was supported by grants from the Institut Curie [grant PICSysBio], the Centre National de la Recherche Scientifique (CNRS), the Ligue Contre le Cancer (Comité de l'Essonne), the Association pour la Recherche sur le Cancer (ARC) [grant number SFI20121205645], the Agence Nationale de la Recherche [grant number ANR-14-CE14-0004-01] and by a fellowship awarded to S.G. by the Ministère de l'Education Nationale, de l'Enseignement Supérieur et de la Recherche and the Association pour la Recherche sur le Cancer [fellowship number DOC20140601310], and Institut Curie [PICSysBio].

Supplementary information

Supplementary information available online at
http://jcs.biologists.org/lookup/doi/10.1242/jcs.187781.supplemental

References

Ababou, M., Dumaire, V., Lécluse, Y. and Amor-Guéret, M. (2002). Bloom's syndrome protein response to ultraviolet-C radiation and hydroxyurea-mediated DNA synthesis inhibition. *Oncogene* **21**, 2079-2088.

Barefield, C. and Karlseder, J. (2012). The BLM helicase contributes to telomere maintenance through processing of late-replicating intermediate structures. *Nucleic Acids Res.* **40**, 7358-7367.

Baumann, C., Körner, R., Hofmann, K. and Nigg, E. A. (2007). PICH, a centromere-associated SNF2 family ATPase, is regulated by Plk1 and required for the spindle checkpoint. *Cell* **128**, 101-114.

Bergoglio, V., Boyer, A.-S., Walsh, E., Naim, V., Legube, G., Lee, M. Y. W. T., Rey, L., Rosselli, F., Cazaux, C., Eckert, K. A. et al. (2013). DNA synthesis by Pol eta promotes fragile site stability by preventing under-replicated DNA in mitosis. *J. Cell Biol.* **201**, 395-408.

Boutros, R. and Ducommun, B. (2008). Asymmetric localization of the CDC25B phosphatase to the mother centrosome during interphase. *Cell Cycle* **7**, 401-406.

Chabosseau, P., Buhagiar-Labarchède, G., Onclercq-Delic, R., Lambert, S., Debatisse, M., Brison, O. and Amor-Guéret, M. (2011). Pyrimidine pool imbalance induced by BLM helicase deficiency contributes to genetic instability in Bloom syndrome. *Nat. Commun.* **2**, 368.

Chan, K.-L., North, P. S. and Hickson, I. D. (2007). BLM is required for faithful chromosome segregation and its localization defines a class of ultrafine anaphase bridges. *EMBO J.* **26**, 3397-3409.

Chan, K. L., Palmai-Pallag, T., Ying, S. and Hickson, I. D. (2009). Replication stress induces sister-chromatid bridging at fragile site loci in mitosis. *Nat. Cell Biol.* **11**, 753-760.

Dai, Y. and Grant, S. (2010). New insights into checkpoint kinase 1 in the DNA damage response signaling network. *Clin. Cancer Res.* **16**, 376-383.

Eykelenboom, J. K., Harte, E. C., Canavan, L., Pastor-Peidro, A., Calvo-Asensio, I., Llorens-Agost, M. and Lowndes, N. F. (2013). ATR activates the S-M checkpoint during unperturbed growth to ensure sufficient replication prior to mitotic onset. *Cell Rep.* **5**, 1095-1107.

Gelot, C., Magdalou, I. and Lopez, B. S. (2015). Replication stress in Mammalian cells and its consequences for mitosis. *Genes* **6**, 267-298.

Gemble, S., Ahuja, A., Buhagiar-Labarchède, G., Onclercq-Delic, R., Dairou, J., Biard, D. S. F., Lambert, S., Lopes, M. and Amor-Guéret, M. (2015). Pyrimidine pool disequilibrium induced by a cytidine deaminase deficiency inhibits PARP-1 activity, leading to the under replication of DNA. *PLoS Genet.* **11**, e1005384.

German, J. (1997). Bloom's syndrome. XX. The first 100 cancers. *Cancer Genet. Cytogenet.* **93**, 100-106.

Hickson, I., Zhao, Y., Richardson, C. J., Green, S. J., Martin, N. M. B., Orr, A. I., Reaper, P. M., Jackson, S. P., Curtin, N. J. and Smith, G. C. M. (2004). Identification and characterization of a novel and specific inhibitor of the ataxia-telangiectasia mutated kinase ATM. *Cancer Res.* **64**, 9152-9159.

Hills, S. A. and Diffley, J. F. X. (2014). DNA replication and oncogene-induced replicative stress. *Curr. Biol.* **24**, R435-R444.

Illuzzi, G., Fouquerel, E., Amé, J.-C., Noll, A., Rehmet, K., Nasheuer, H.-P., Dantzer, F. and Schreiber, V. (2014). PARG is dispensable for recovery from transient replicative stress but required to prevent detrimental accumulation of poly(ADP-ribose) upon prolonged replicative stress. *Nucleic Acids Res.* **42**, 7776-7792.

Katsuragi, Y. and Sagata, N. (2004). Regulation of Chk1 kinase by autoinhibition and ATR-mediated phosphorylation. *Mol. Biol. Cell* **15**, 1680-1689.

Langelier, M.-F. and Pascal, J. M. (2013). PARP-1 mechanism for coupling DNA damage detection to poly(ADP-ribose) synthesis. *Curr. Opin. Struct. Biol.* **23**, 134-143.

Lecona, E. and Fernández-Capetillo, O. (2014). Replication stress and cancer: it takes two to tango. *Exp. Cell Res.* **329**, 26-34.

Liu, Q., Guntuku, S., Cui, X. S., Matsuoka, S., Cortez, D., Tamai, K., Luo, G., Carattini-Rivera, S., DeMayo, F., Bradley, A. et al. (2000). Chk1 is an essential

Journal of Cell Science

kinase that is regulated by Atr and required for the G(2)/M DNA damage checkpoint. *Genes Dev.* **14**, 1448-1459.

Luo, X. and Kraus, W. L. (2012). On PAR with PARP: cellular stress signaling through poly(ADP-ribose) and PARP-1. *Genes Dev.* **26**, 417-432.

Magdalou, I., Lopez, B. S., Pasero, P. and Lambert, S. A. E. (2014). The causes of replication stress and their consequences on genome stability and cell fate. *Semin. Cell Dev. Biol.* **30**, 154-164.

Mazouzi, A., Velimezi, G. and Loizou, J. I. (2014). DNA replication stress: causes, resolution and disease. *Exp. Cell Res.* **329**, 85-93.

Min, W., Bruhn, C., Grigaravicius, P., Zhou, Z. W., Li, F., Krüger, A., Siddeek, B., Greulich, K. O., Popp, O., Meisezahl, C. et al. (2013). Poly(ADP-ribose) binding to Chk1 at stalled replication forks is required for S-phase checkpoint activation. *Nat. Commun.* **4**, 2993.

Naim, V., Wilhelm, T., Debatisse, M. and Rosselli, F. (2013). ERCC1 and MUS81-EME1 promote sister chromatid separation by processing late replication intermediates at common fragile sites during mitosis. *Nat. Cell Biol.* **15**, 1008-1015.

Ng, C.-P., Lee, H. C., Ho, C. W., Arooz, T., Siu, W. Y., Lau, A. and Poon, R. Y. C. (2004). Differential mode of regulation of the checkpoint kinases CHK1 and CHK2 by their regulatory domains. *J. Biol. Chem.* **279**, 8808-8819.

Nygaard, P. (1986). On the role of cytidine deaminase in cellular metabolism. *Adv. Exp. Med. Biol.* **195**, 415-420.

Petermann, E. and Caldecott, K. W. (2006). Evidence that the ATR/Chk1 pathway maintains normal replication fork progression during unperturbed S phase. *Cell Cycle* **5**, 2203-2209.

Raab, M., Krämer, A., Hehlgans, S., Sanhaji, M., Kurunci-Csacsko, E., Dötsch, C., Bug, G., Ottmann, O., Becker, S. and Pachl, F. (2015). Mitotic arrest and slippage induced by pharmacological inhibition of Polo-like kinase 1. *Mol. Oncol.* **9**, 140-154.

Rudolph, D., Steegmaier, M., Hoffmann, M., Grauert, M., Baum, A., Quant, J., Haslinger, C., Garin-Chesa, P. and Adolf, G. R. (2009). BI 6727, a Polo-like kinase inhibitor with improved pharmacokinetic profile and broad antitumor activity. *Clin. Cancer Res.* **15**, 3094-3102.

Sancar, A., Lindsey-Boltz, L. A., Ünsal-Kaçmaz, K. and Linn, S. (2004). Molecular mechanisms of mammalian DNA repair and the DNA damage checkpoints. *Annu. Rev. Biochem.* **73**, 39-85.

Savino, T. M., Gébrane-Younès, J., De Mey, J., Sibarita, J.-B. and Hernandez-Verdun, D. (2001). Nucleolar assembly of the rRNA processing machinery in living cells. *J. Cell Biol.* **153**, 1097-1110.

Segurado, M. and Tercero, J. A. (2009). The S-phase checkpoint: targeting the replication fork. *Biol. Cell* **101**, 617-627.

Serdjebi, C., Milano, G. and Ciccolini, J. (2015). Role of cytidine deaminase in toxicity and efficacy of nucleosidic analogs. *Expert Opin. Drug Metab. Toxicol.* **11**, 665-672.

Smits, V. A. J. and Gillespie, D. A. (2015). DNA damage control: regulation and functions of checkpoint kinase 1. *FEBS J.* **282**, 3681-3692.

Tallis, M., Morra, R., Barkauskaite, E. and Ahel, I. (2014). Poly(ADP-ribosyl)ation in regulation of chromatin structure and the DNA damage response. *Chromosoma* **123**, 79-90.

Tse, A. N., Rendahl, K. G., Sheikh, T., Cheema, H., Aardalen, K., Embry, M., Ma, S., Moler, E. J., Ni, Z. J., Lopes de Menezes, D. E. et al. (2007). CHIR-124, a novel potent inhibitor of Chk1, potentiates the cytotoxicity of topoisomerase I poisons in vitro and in vivo. *Clin. Cancer Res.* **13**, 591-602.

Ye, F.-G., Song, C.-G., Cao, Z.-G., Xia, C., Chen, D.-N., Chen, L., Li, S., Qiao, F., Ling, H., Yao, L. et al. (2015). Cytidine deaminase axis modulated by miR-484 differentially regulates cell proliferation and chemoresistance in breast cancer. *Cancer Res.* **75**, 1504-1515.

Ying, S., Minocherhomji, S., Chan, K. L., Palmai-Pallag, T., Chu, W. K., Wass, T., Mankouri, H. W., Liu, Y. and Hickson, I. D. (2013). MUS81 promotes common fragile site expression. *Nat. Cell Biol.* **15**, 1001-1007.

Zauri, M., Berridge, G., Thézénas, M.-L., Pugh, K. M., Goldin, R., Kessler, B. M. and Kriaucionis, S. (2015). CDA directs metabolism of epigenetic nucleosides revealing a therapeutic window in cancer. *Nature* **524**, 114-118.

Zhao, H. and Piwnica-Worms, H. (2001). ATR-mediated checkpoint pathways regulate phosphorylation and activation of human Chk1. *Mol. Cell. Biol.* **21**, 4129-4139.

Zuazua-Villar, P., Rodriguez, R., Gagou, M. E., Eyers, P. A. and Meuth, M. (2014). DNA replication stress in CHK1-depleted tumour cells triggers premature (S-phase) mitosis through inappropriate activation of Aurora kinase B. *Cell Death Dis.* **5**, e1253.

Supplementary Figures

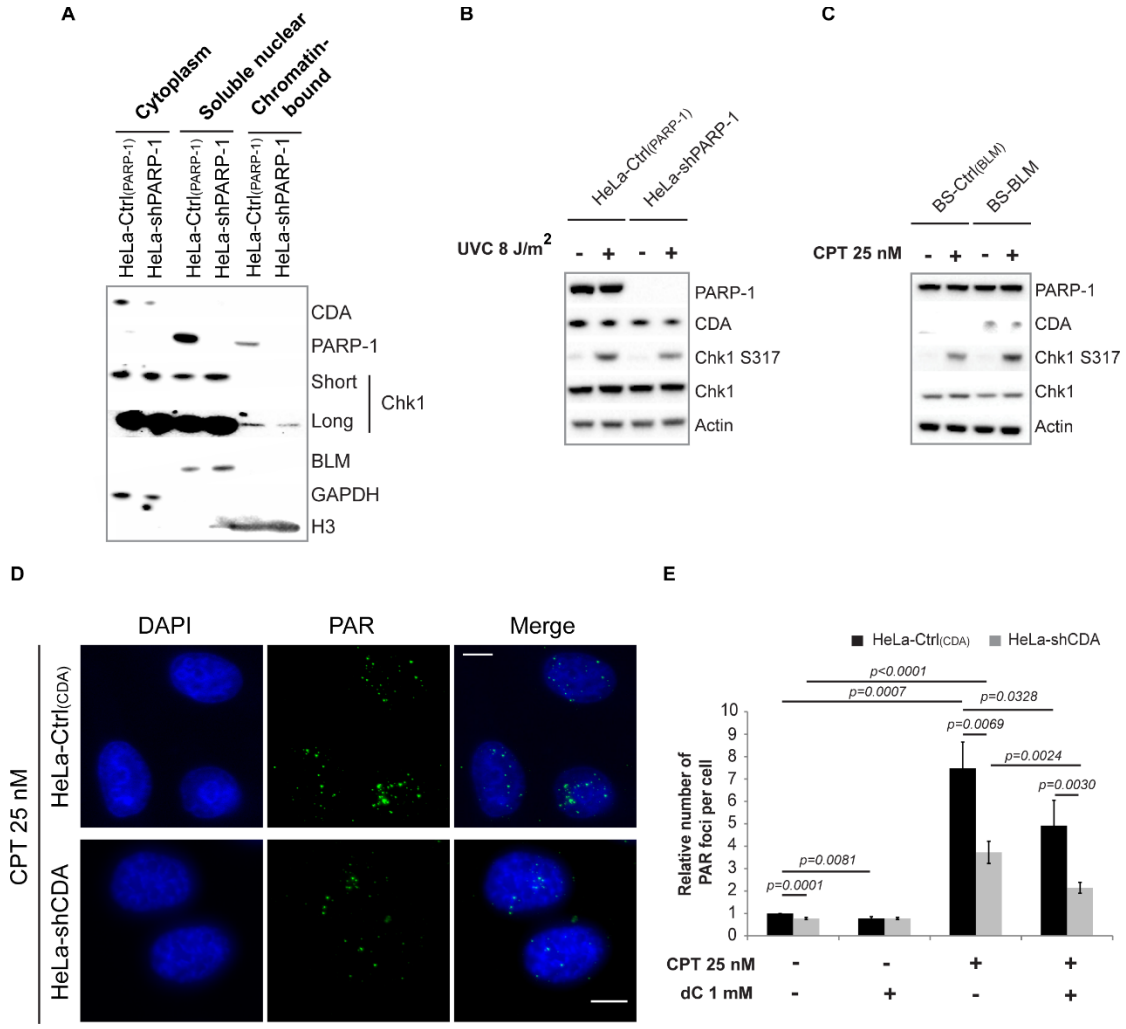

Figure S1 (related to Figure 1): CDA deficiency jeopardizes the activation of PARP-1 and Chk1 after genotoxic stress

(A) Representative immunoblot of subcellular fractions of HeLa-Ctrl$_{(PARP-1)}$ and HeLa-shPARP-1 cells. The GAPDH, BLM and H3 proteins were used as loading controls for the cytoplasm, nucleus and chromatin-bound fractions, respectively. (B) Representative immunoblot of HeLa-Ctrl$_{(PARP-1)}$ and HeLa-shPARP-1 cells left unexposed or exposed to 8 J/m^2 UVC. (C) Representative immunoblot of BS-Ctrl$_{(BLM)}$ or BS-BLM cells left untreated or treated with 25 nM CPT for 8 hours. (D) Representative immunofluorescence deconvoluted z-projection images of HeLa-Ctrl$_{(CDA)}$ (upper panel) and HeLa-shCDA (lower panel) cells treated with 25 nM CPT. Nuclei were visualized by staining with DAPI (in blue). PAR foci were stained with an antibody specific for PAR (in green). Scale bar: 5 µm. (E) Relative numbers of PAR foci in HeLa-Ctrl$_{(CDA)}$ and HeLa-shCDA cells pretreated with 1 mM dC and left untreated or treated with 25 nM CPT (n=4, >410 cells analyzed). The error bars represent the mean ± SD. Statistical significance was calculated with Student's t-test.

Journal of Cell Science • Supplementary information

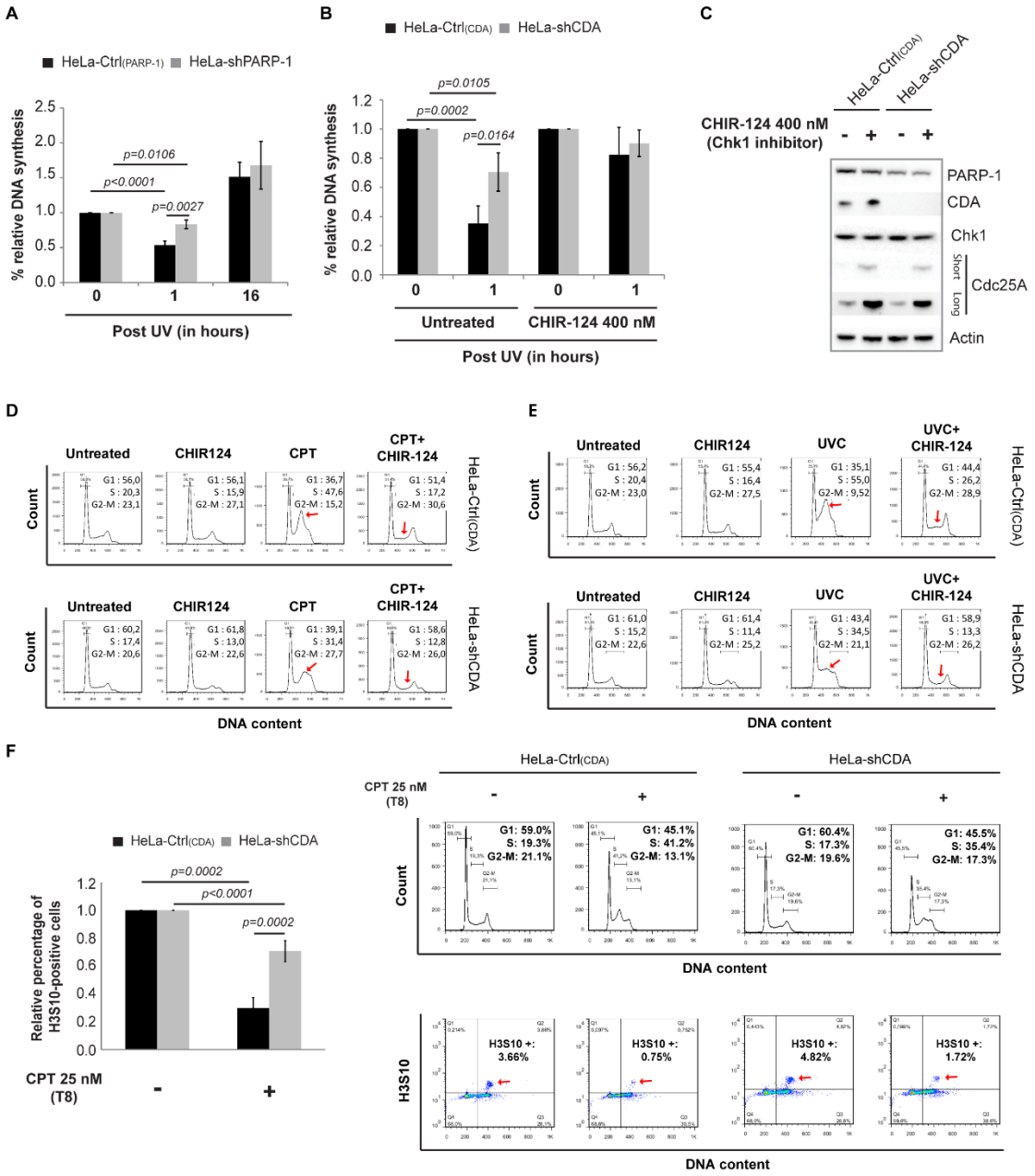

Figure S2 (related to Figure 2): The Chk1-dependent halting of DNA synthesis is reduced in PARP-1- and CDA-deficient cells

(A) Percentage relative DNA synthesis in HeLa-Ctrl$_{(PARP-1)}$ (black bars) and HeLa-shPARP-1 (gray bars) cells with and without exposure to 8 J/m^2 UVC (n=4). (B) Percentage relative DNA synthesis in HeLa-Ctrl$_{(CDA)}$ (black bars) or HeLa-shCDA (gray bars) cell lines after pretreatment with 400 nM CHIR-124, with and without exposure to 8 J/m^2 UVC (n=3). (C) Representative immunoblot of HeLa-Ctrl$_{(CDA)}$ and HeLa-shCDA cells left untreated or treated with 400 nM CHIR-124 for 8 hours. (D-E) Percentage of HeLa-Ctrl$_{(CDA)}$ (black bars) and HeLa-shCDA (gray bars) cells in S-phase, with and without treatment with 400 nM CHIR-124 and/or (D) 25 nM CPT (n=3) or (E) 8 J/m^2 UVC (n=3). (F) Left panel – Relative

Journal of Cell Science • Supplementary information

percentage of H3S10-positive cells in HeLa-Ctrl$_{(CDA)}$ (black bars) and HeLa-shCDA (gray bars) left untreated or treated with 25 nM CPT for 8 hours (n=4). Right panel – Representative images of H3S10-positive cells quantified by flow cytometry. Error bars represent the mean ± SD. Statistical significance was calculated with Student's t-test.

Journal of Cell Science • Supplementary information

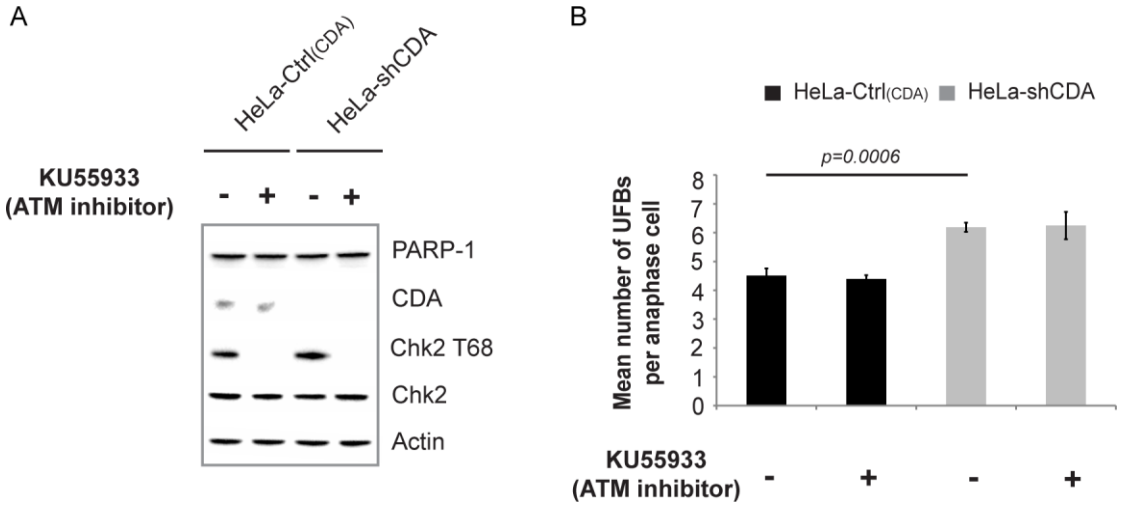

Figure S3 (related to Figure 3): ATM-Chk2 pathway is not involved in UFB formation

(A) Representative immunoblot of HeLa-Ctrl$_{(CDA)}$ and HeLa-shCDA cells left untreated or treated with 10 µM KU55933 for 8 hours. (B) Mean number of UFBs per anaphase cell in HeLa-Ctrl$_{(CDA)}$ (black bars) and HeLa-shCDA (gray bars) cells left untreated or treated with 10 µM KU55933 for 8 hours (n=3; >80 anaphase cells analyzed). Error bars represent the mean ± SD. Statistical significance was calculated with Student's t-test.

Journal of Cell Science • Supplementary information

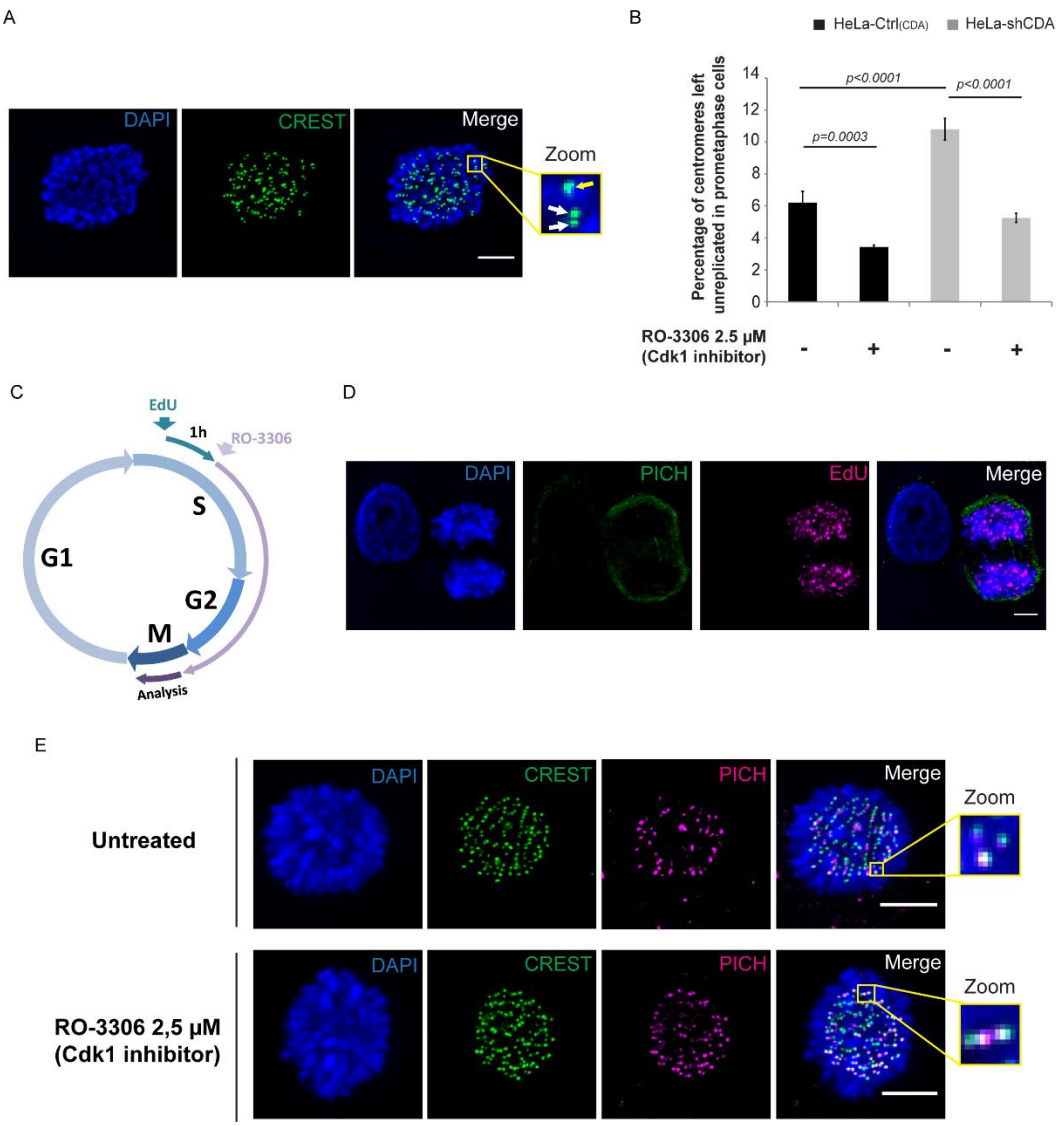

Figure S4 (related to Figure 4): Promoting the completion of DNA replication decreases the percentage of unreplicated centromeres in mitosis

(A) Representative deconvoluted z-projection immunofluorescence images of prometaphase HeLa cells. DNA was visualized by staining with DAPI (in blue). Centromeres were stained with a CREST antibody (in green). The boxed images are enlargements; single-dotted CREST foci are indicated by yellow arrows and double-dotted CREST foci are indicated by white arrows. (B) Percentage of centromeres left unreplicated in HeLa-Ctrl$_{(CDA)}$ and HeLa-shCDA cells with and without treatment with 2.5 µM RO-3306 for 6 hours (n=4; >120 metaphase cells analyzed). (C) Schematic representation of EdU incorporation before the addition of RO-3306 during the cell cycle; all cells analyzed during mitosis had incorporated EdU. (D) Representative deconvoluted z-projection immunofluorescence images of HeLa EdU-positive

mitotic cells. DNA was visualized by staining with DAPI (in blue). UFB was stained with an anti-PICH antibody (in green). EdU was stained with Alexa Fluor 555 (in magenta). (E) Representative deconvoluted z-projection immunofluorescence images of prometaphase HeLa cells left untreated or treated with 2.5 µM RO-3306 for 6 hours. DNA was visualized by staining with DAPI (in blue). PICH was stained with Alexa Fluor 555 (in magenta) and centromeres were stained with a CREST antibody (in green). The boxed images are enlargements showing the colocalization of PICH with centromeres. Error bars represent the mean ± SD. Statistical significance was calculated with Student's *t*-test. Scale bar: 5 µm.

Journal of Cell Science • Supplementary information